

WR 120bb and WR 120bc: a pair of WN9h stars with possibly interacting circumstellar shells

S. Burgemeister^{1*}, V. V. Gvaramadze^{2,3*}, G. S. Stringfellow^{4*†}, A. Y. Kniazev^{5,6,2*}, H. Todt^{1*}, and W.-R. Hamann^{1*}

¹*Institute for Physics and Astronomy, University Potsdam, 14476 Potsdam, Germany*

²*Sternberg Astronomical Institute, Lomonosov Moscow State University, Universitetskij Pr. 13, Moscow 119992, Russia*

³*Isaac Newton Institute of Chile, Moscow Branch, Universitetskij Pr. 13, Moscow 119992, Russia*

⁴*Center for Astrophysics and Space Astronomy, University of Colorado, 389 UCB Boulder, Colorado 80309-0389, USA*

⁵*South African Astronomical Observatory, PO Box 9, 7935 Observatory, Cape Town, South Africa*

⁶*Southern African Large Telescope Foundation, PO Box 9, 7935 Observatory, Cape Town, South Africa*

ABSTRACT

Two optically obscured Wolf-Rayet (WR) stars have been recently discovered by means of their infrared (IR) circumstellar shells, which show signatures of interaction with each other. Following the systematics of the WR star catalogues, these stars obtain the names WR 120bb and WR 120bc. In this paper, we present and analyse new near-IR, *J*, *H*, and *K*-band, spectra using the Potsdam Wolf-Rayet (PoWR) model atmosphere code. For that purpose, the atomic data base of the code has been extended in order to include all significant lines in the near-IR bands.

The spectra of both stars are classified as WN9h. As their spectra are very similar the parameters that we obtained by the spectral analyses hardly differ. Despite their late spectral subtype, we found relatively high stellar temperatures of 63 kK. The wind composition is dominated by helium, while hydrogen is depleted to 25 per cent by mass.

Because of their location in the Scutum-Centaurus arm, WR 120bb and WR 120bc appear highly reddened, $A_{K_s} \approx 2$ mag. We adopt a common distance of 5.8 kpc to both stars, which complies with the typical absolute *K*-band magnitude for the WN9h subtype of -6.5 mag, is consistent with their observed extinction based on comparison with other massive stars in the region, and allows for the possibility that their shells are interacting with each other. This leads to luminosities of $\log(L/L_\odot) = 5.66$ and 5.54 for WR 120bb and WR 120bc, with large uncertainties due to the adopted distance.

The values of the luminosities of WR 120bb and WR 120bc imply that the immediate precursors of both stars were red supergiants (RSG). This implies in turn that the circumstellar shells associated with WR 120bb and WR 120bc were formed by interaction between the WR wind and the dense material shed during the preceding RSG phase.

Key words: line: identification – circumstellar matter – stars: fundamental parameters – stars: massive – stars: Wolf-Rayet.

1 INTRODUCTION

Wolf-Rayet (WR) stars play a key role in the cosmic circuit of matter. As they are massive hot stars with a strong stellar wind, they continuously enrich their environment with metals and ionise the surrounding interstellar matter. Furthermore, they are considered as progenitors of supernovae and γ -ray bursts. Nevertheless, the origin of WR stars is not yet safely established and their physics is far from being

* E-mail: sburgem@astro.physik.uni-potsdam.de (SB); vgvaram@mx.iki.rssi.ru (VVG); Guy.Stringfellow@colorado.edu (GSS); akniazev@sao.ac.za (AYK); htodt@astro.physik.uni-potsdam.de (HT); wrh@astro.physik.uni-potsdam.de (WRH)

† Observations obtained with the Apache Point Observatory 3.5-meter telescope, which is owned and operated by the Astrophysical Research Consortium.

fully understood. Detection and study of new WR stars is therefore warranted.

Until recently, the main channel for detection of WR stars was through narrow-band optical surveys (e.g. Shara et al. 1999, and references therein). The advent of infrared (IR) observations brought new possibilities. Searches for new WR stars using narrow-band mid-IR surveys (Shara et al. 2009, 2012) and IR colour-based selection of objects (Hadfield et al. 2007; Mauerhan et al. 2011) led to the almost two-fold increase of the known Galactic population of these stars.

Another important tool for revealing WR and other types of evolved massive stars is through detection of their circumstellar nebulae. Classically it is known that some WR stars exhibit ring nebulae that are emitting in $H\alpha$ and other optical lines (Johnson & Hogg 1965; Chu et al. 1983; Dopita et al. 1994; Marston 1995). Because of the high obscuration in the Galactic plane (where most sites of massive star formation are located) the distant WR nebulae can be detected mainly through their mid- and far-IR emission (e.g. van Buren & McCray 1988; Marston 1991; Mathis et al. 1992), whose origin can be attributed to radiatively heated circumstellar dust (van Buren & McCray 1988; Marston 1991).

Barniske, Oskinova, & Hamann (2008) found a nebula around the WN9h star WR102ka in the Galactic Centre region. They obtained a high-resolution IR spectrum of the nebula and analysed the emission from warm dust and molecules. To our knowledge, this was the first unambiguous detection of a dusty nebula around a WN star (cf. Flagey et al. 2011).

Searches for circumstellar nebulae around evolved massive stars with the old generation of IR telescopes (onboard the *Infrared Astronomical Satellite*, the *Infrared Space Observatory* and the *Midcourse Space Experiment satellite*), led to the detection of a number of objects (e.g. Marston 1991; Trams et al. 1998; Voors et al. 2000; Egan et al. 2002; Clark et al. 2003), some of which were already known from optical and/or radio observations. Significant progress in detection of new circumstellar nebulae was achieved with the release of the MIPS GAL and other *Spitzer Space Telescope* Legacy Programmes. Using *Spitzer* data, several groups independently discovered many dozens of circumstellar shells (Gvaramadze et al. 2010a; Mizuno et al. 2010; Wachter et al. 2010), while follow-up spectroscopy of the central stars of these shells led to the discovery of dozens of WR, luminous blue variable, and other massive stars (Gvaramadze et al. 2009, 2010a,b,c, 2011; Wachter et al. 2010, 2011; Mauerhan et al. 2010; Stringfellow et al. 2011, 2012).

Two WR stars revealed with *Spitzer* via detection of their circumstellar shells are the subject of this paper. The WR nature of these stars (formerly known as 2MASS J18420630-0348224 and 2MASS J18420827-351039) were identified by Mauerhan et al. (2010) by means of IR spectroscopy. In the systematics of the Galactic WR star catalogue (van der Hucht 2001, 2006)¹, we call these stars WR120bb and WR120bc in the rest of the paper. Mauerhan et al. (2010) also identified two more evolved massive stars (of spectral types of WC8 and O7–8 III–I), which along

with WR120bb and WR120bc form a previously unknown star cluster, provided they lie at similar distances.

Analyses of WR stars are preferably based on their optical and ultraviolet spectra, which are not accessible for WR120bb and WR120bc because of high interstellar extinction. However, attempts to constrain the basic parameters of WR stars on basis of their *K*-band spectra alone have been made (e.g. Barniske et al. 2008; Liermann et al. 2010). In the present paper the addition of the *J* and *H*-bands are included along with the *K*-band analysis, which turn out to be very valuable.

The rest of the paper is organised as follows. In Section 2 we introduce WR120bb and WR120bc and their circumstellar nebulae in more detail. Section 3 describes our spectroscopic observations. After a short characterisation of the Potsdam Wolf-Rayet (PoWR) model atmospheres, the spectra are quantitatively analysed in Section 4. The evolutionary status of the stars and the origin of their nebulae are discussed in Section 5. We summarise our findings in Section 6.

2 THE CIRCUMSTELLAR SHELLS MN85 AND MN86 AND THEIR CENTRAL STARS

Fig. 1 (left panel) shows the $24\ \mu\text{m}$ image of two adjacent circular shells and their central stars (indicated by circles). The shells were discovered in the course of our search for evolved massive stars via detection of their circumstellar nebulae in the archival data of the *Spitzer* Legacy Programmes (for motivation and the results of this search see Gvaramadze et al. 2010a). The image was obtained with the Multiband Imaging Photometer for *Spitzer* (MIPS; Rieke et al. 2004) within the framework of the 24 and 70 Micron Survey of the Inner Galactic Disc with MIPS (MIPSGAL; Carey et al. 2009). We have called the shells MN85 and MN86² (Gvaramadze et al. 2010a). One of the shells (MN86) can also be seen at $70\ \mu\text{m}$ (see fig. 1 in Mauerhan et al. 2010). Both shells were also covered by the Galactic Legacy Infrared Mid-Plane Survey Extraordinaire (GLIMPSE; Benjamin et al. 2003) carried out with the Infrared Array Camera (IRAC; Fazio et al. 2004) and the Mid-Infrared All Sky Survey carried out with the *Wide-field Infrared Survey Explorer* (*WISE*; Wright et al. 2010). The first survey provides images at 3.6, 4.5, 5.8 and $8\ \mu\text{m}$, and the second one at 3.4, 4.6, 12 and $22\ \mu\text{m}$. The shells are invisible in the IRAC wavebands, but both can be seen in the *WISE* $22\ \mu\text{m}$ image (not shown here). There is also a hint of $12\ \mu\text{m}$ emission probably associated with the nebulae (second left panel of Fig. 1). In Fig. 1 (second panel from the right) we also show the *WISE* $3.4\ \mu\text{m}$ image of the same field, where the central stars of MN85 and MN86 are indicated by circles and the WC8 and O7–8 III–I stars (see Section 1) are marked by diamonds.

MN85 and MN86 were also covered by the Multi-Array Galactic Plane Imaging Survey (MAGPIS; Helfand et al. 2006) carried out with the Very Large Array (VLA). Fig. 1 (right panel) shows that the shell MN86 has a clear radio counterpart at 20 cm.

¹ See updated version of this catalogue on <http://pacrowther.staff.shef.ac.uk/WRcat>

² In the SIMBAD data base the shells are named [GKF2010] MN85 and [GKF2010] MN86.

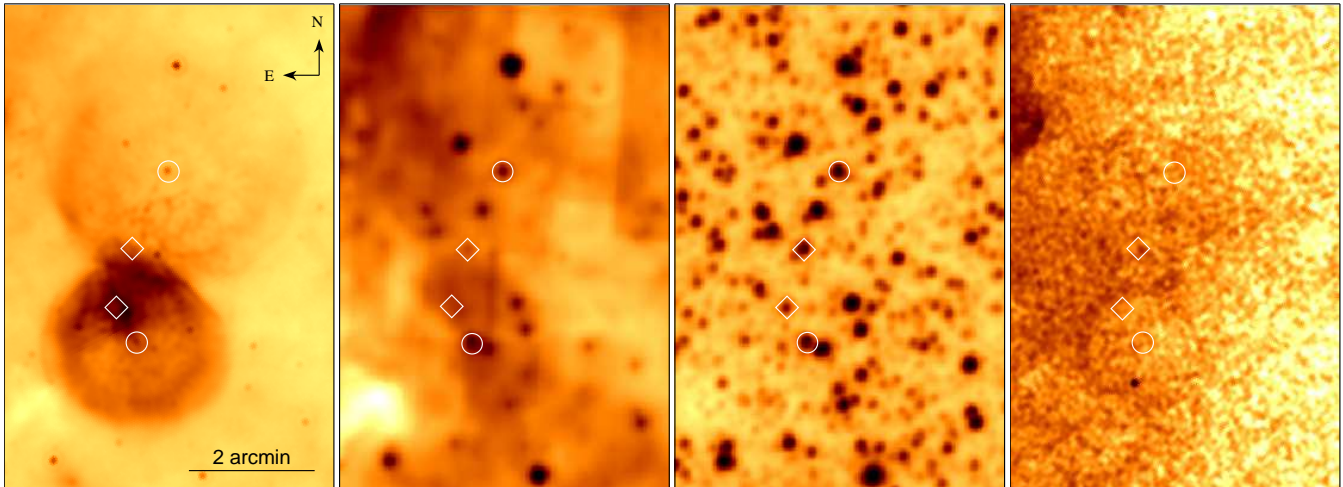


Figure 1. From left to right: images at $24\ \mu\text{m}$ (MIPS), $12\ \mu\text{m}$ (WISE), $3.4\ \mu\text{m}$ (WISE), and 20 cm (VLA) of the field containing the two interacting nebulae MN85 and MN86. The positions of the central (WN9h) stars of the nebulae are marked by circles, while two other massive stars (WC8 and O7–8III–I) are indicated by diamonds (see text for details).

The MIPS $24\ \mu\text{m}$ image shows that both shells are brightest where the two shells apparently overlap, which might be caused by the interaction between the radially expanding shells (cf. Gvaramadze et al. 2010a; Wachter et al. 2010). Indeed, Mauerhan et al. (2010) showed that the overlapping region of the shells is significantly brighter than the sum of the surface brightnesses of the neighbouring parts of the shells, which indicates that it is intrinsically bright emission. The enhanced brightness of this region can also be seen in the $70\ \mu\text{m}$ image of the shells in fig. 1 in Mauerhan et al. (2010). If the shells are indeed interacting with each other, then their almost circular shape implies that they came in contact only recently. The existing data, however, do not allow us to unambiguously assert that the physical contact between the shells is real.

The angular radius of the larger shell (MN85) is $\simeq 1.9$ arcmin, while that of MN86 is $\simeq 1.5$ arcmin. In Section 4.3 we argue that the distance to the objects is ~ 6 kpc, so that the linear radius of MN85 and MN86 is ~ 3 pc. Circumstellar shells of this size are typical of late WN-type (WNL) stars and luminous blue variables. The possible origin of MN85 and MN86 are discussed in Section 5.

The central location of point sources indicated in Fig. 1 by circles suggests that they might be associated with the nebulae. This possibility is supported by the position of these stars in the colour-colour diagrams by Hadfield et al. (2007), where they fall in the region populated by WR stars. The details of the central stars are summarised in Table 1. The coordinates and the J , H , K_s magnitudes are taken from the 2MASS (Two Micron All Sky Survey) All-Sky Catalog of Point Sources (Cutri et al. 2003). The I magnitudes are from the DENIS (Deep Near Infrared Survey of the Southern Sky) data base (The DENIS Consortium 2005), the IRAC magnitudes are from the GLIMPSE Source Catalogue (I + II + 3D), and the WISE 12 and $22\ \mu\text{m}$ magnitudes are from the WISE All-Sky Data Release (Cutri et al. 2012).

Table 1. Details of the central stars associated with the nebulae MN85 and MN86.

	WR 120bb (MN85)	WR 120bc (MN86)
RA(J2000)	$18^{\text{h}}42^{\text{m}}06^{\text{s}}.31$	$18^{\text{h}}42^{\text{m}}08^{\text{s}}.27$
Dec(J2000)	$-03^{\circ}48'22''.5$	$-03^{\circ}51'02''.9$
l	$28^{\circ}4811$	$28^{\circ}4452$
b	$0^{\circ}3371$	$0^{\circ}3094$
I (mag)	17.61 ± 0.14	16.96 ± 0.10
J (mag)	11.95 ± 0.03	11.85 ± 0.03
H (mag)	10.22 ± 0.02	10.26 ± 0.03
K_s (mag)	9.16 ± 0.02	9.27 ± 0.03
[3.6] (mag)	8.28 ± 0.04	8.43 ± 0.04
[4.5] (mag)	7.63 ± 0.04	7.88 ± 0.05
[5.8] (mag)	7.43 ± 0.03	7.67 ± 0.03
[8.0] (mag)	7.04 ± 0.03	7.20 ± 0.03
[12.0] (mag)	6.92 ± 0.04	6.96 ± 0.04
[22.0] (mag)	5.23 ± 0.05	3.85 ± 0.06

All these catalogues and data bases are accessible through the Gator engine³.

3 SPECTROSCOPIC OBSERVATIONS AND DATA REDUCTION

Observations were carried out with the Apache Point Observatory (APO) 3.5m telescope using the medium-resolution infrared spectrograph TripleSpec (Wilson et al. 2004), which provides coverage from 0.95 to $2.46\ \mu\text{m}$ in five orders with a resolving power of about 3200 using a $1''.1 \times 43''$ slit. The exposures were obtained in a nodded ABBA sequence offset along the slit by 20 arcsec to facilitate sky subtraction and to allow for the correction of detector artifacts. The slit was aligned along the east-west sky projection. WR 120bb was observed on 2010 May 19 UT at an airmass of ~ 1.55 with

³ <http://irsa.ipac.caltech.edu/applications/Gator/>

a seeing of ~ 1 arcsec, and WR 120bc on 2010 May 30 UT at an airmass of 1.7 with ~ 1.2 arcsec seeing. Peak counts in the strongest emission lines for both stars remained below $\sim 14,000$ counts, corresponding to a detector non-linearity of < 0.1 per cent.

Flat fielding was performed using dome flat lamps, and wavelength calibration utilized the OH sky lines obtained during the exposures. Sky subtraction, flat fielding, wavelength calibration, and extraction of the spectra were achieved using a modified version of the software package `xspextool` (originally developed for use with SpeX on the NASA Infrared Telescope Facility (IRTF); Cushing, Vacca, & Rayner 2004) redesigned for use with the APO Triple-Spec specific instrument characteristics. Final wavelength calibration in each order resulted in an RMS error of < 1.2 Å for WR 120bb, and < 1.5 Å for WR 120bc. The A0 V star HD 171149 was observed immediately before or after observing each star for use in performing the telluric and flux corrections. The difference in airmass between the telluric and programme stars were < 0.06 . Telluric corrections and approximate flux calibrations were performed with the IDL routine `xtellcor` that implements the method developed and described by Vacca, Cushing, & Rayner (2003).

The resulting combined spectrum of WR 120bb has a typical signal-to-noise ratio (S/N) in the continuum of ≈ 100 , 60, and 4–18 in the *K*, *H*, and *J*-bands, respectively. Likewise, the values for the combined spectrum for WR 120bc are 250, 200, and 6–75. The stars are heavily reddened, resulting in the much lower S/N at shorter wavelengths.

4 WR 120bb AND WR 120bc: TWO ALMOST IDENTICAL WN9h STARS

4.1 Spectral type

In Figs. 2 and 3 we present the *J*, *H*, and *K*-band spectra of WR 120bb and WR 120bc. The spectra are very similar to each other and show numerous emission lines of H I, He I and He II. Hydrogen lines are generally blended with the corresponding He II lines. We also detect emissions of N III and N IV. The absence of carbon and oxygen lines indicate that both stars belong to the nitrogen (WN) sequence of the WR stars. To determine the subtypes of WR 120bb and WR 120bc more precisely, we use the equivalent width (EW) ratios: $\text{EW}(\text{He II } 1.012)/\text{EW}(\text{He I } 1.083)$ and $\text{EW}(\text{He II } 2.189)/\text{EW}(\text{He II } + \text{Br}\gamma)$ (see Crowther et al. 2006, and Table 5 therein). Following Crowther et al. (2006), WN stars belong to the subtype WN8 if the equivalent width ratio $\text{EW}(\text{He II } 1.012)/\text{EW}(\text{He I } 1.083)$ is between 0.07 and 0.2 and if $\text{EW}(\text{He II } 2.189)/\text{EW}(\text{He II } + \text{Br}\gamma)$ is between 0.1 and 0.4. If the equivalent width ratios are below these values, the stars belong to the subtype WN9. If we compare these ratios with the values that we found for WR 120bb and WR 120bc (see Table 2), we can assign the two stars to the WN9 subtype. Following the three-dimensional classification for WN stars by Smith, Shara, & Moffat (1996), we add a suffix ‘h’ to WN9 to indicate the presence of hydrogen emission lines, so that WR 120bb and WR 120bc are WN9h stars. This result only slightly differs from that of Mauerhan et al. (2010), who assigned both stars to the WN8-9h subtype.

Table 2. Equivalent widths (EWs; in Å) of emission lines and their ratios used for spectral classification of WR 120bb and WR 120bc.

EW	WR 120bb	WR 120bc
He II 1.012	28.3 \pm 7.4	31.3 \pm 2.8
He I 1.083	555.5 \pm 10.4	478.1 \pm 9.3
He II + Br γ	122.2 \pm 1.0	122.0 \pm 1.1
He II 2.189	3.4 \pm 0.3	5.0 \pm 0.2
EW(He II 1.012)/EW(He I 1.083)	0.051	0.065
EW(He II 2.189)/EW(He II + Br γ)	0.028	0.041

4.2 Spectral analysis and stellar parameters

To analyse the stellar spectra and to derive the fundamental parameters of WR 120bb and WR 120bc, the PoWR models for expanding stellar atmospheres are used. These models account for complex model atoms including iron-line blanketing in non-LTE (for a detailed description see Gräfener et al. 2002; Hamann & Gräfener 2003, 2004). For the analysis of the near-IR spectra, the model atom of H I had to be extended compared to the model grid for WNL-stars (Hamann & Gräfener 2004) in order to reproduce the Brackett-lines in the *H*-band. Other extended model atoms are He I, He II, N III and N IV. The new atomic data are taken from the NIST Atomic Spectra Database (Kramida et al. 2012) and from the Atomic Line List (van Hoof 1999).

The normalised emission line spectra of WR stars depend on two principal parameters: the stellar temperature, T_* , and the so-called transformed radius, R_t . The stellar temperature T_* denotes the effective temperature, which is related to the stellar radius R_* and the bolometric luminosity L via the Stefan-Boltzmann law $L = 4\pi R_*^2 \sigma T_*^4$, where σ is the Stefan-Boltzmann constant and R_* is by definition the radius where the Rosseland optical depth reaches 20. Alternatively, one may quote the radius where the Rosseland mean optical depth of the stellar wind is $\tau_R = 2/3$. Since the winds of our two program stars are very dense, this “pseudo-photosphere” is located far out in the wind, at about $3.5 R_*$ (see Table 3). Related to that radius, the effective temperature $T_{2/3}$ is much lower than T_* (see Table 3).

The transformed radius R_t is related to the mass-loss rate \dot{M} and defined by

$$R_t = R_* \left[\frac{v_\infty}{2500 \text{ km s}^{-1}} \bigg/ \frac{\sqrt{D} \dot{M}}{10^{-4} \text{ M}_\odot \text{ yr}^{-1}} \right]^{2/3}, \quad (1)$$

introducing the clumping contrast D and the terminal velocity of the wind v_∞ .

In order to achieve a good fit of the electron scattering wings, we set $D = 10$. This is consistent with recent discussions of clumping (see Hamann, Feldmeier, & Oskinova 2008). Note that the effect of D is simply a scaling of the empirically derived mass-loss rate, which is proportional to $D^{-1/2}$.

For the velocity field of the wind we adopt the usual

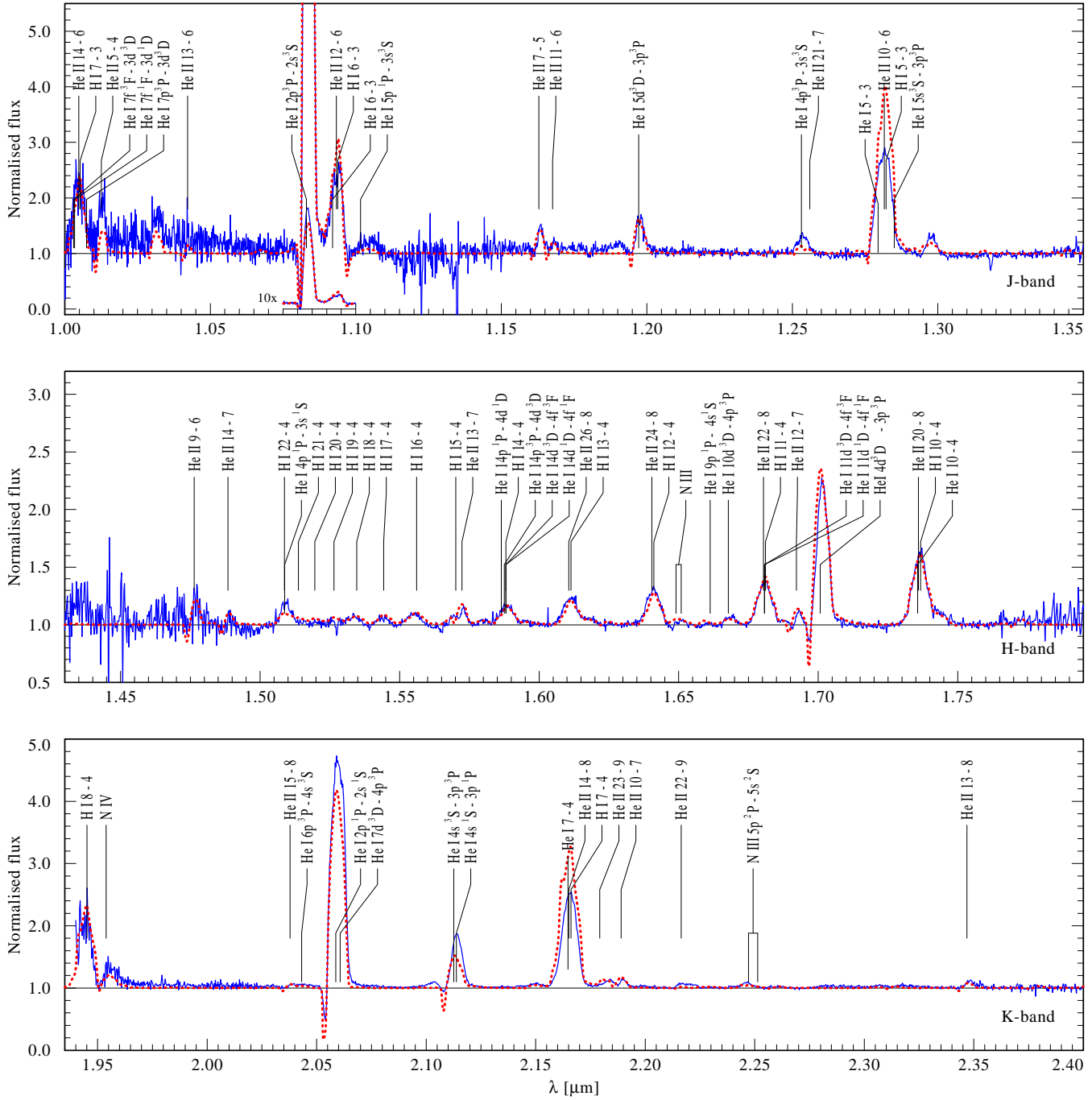


Figure 2. Observed J , H , and K -band spectra (blue-solid line) of WR120bb, compared with the best-fitting model (red-dotted line) with the parameters as given in Table 3. For normalisation the observed spectra were divided by the reddened model continuum, and then slightly aligned “by eye” for an exact match of the continuum slope.

β -law, with the terminal velocity v_∞ being a free parameter. The exponent β is set to unity throughout this work.

The basic model parameters T_* and R_t are derived from fitting the lines of the model spectra to the lines in the normalised observed spectra (see Figs. 2 and 3). The normalisation is achieved by dividing the flux calibrated observed spectra by the theoretical continuum.

For a systematic determination of those models which fit the observations best, we calculated a small grid of models

in the $T_* - R_t$ parameter plane. The terminal wind velocity is $v_\infty = 750 \text{ km s}^{-1}$, as inferred from the P-Cygni like line profiles of the He I lines at $1.70 \text{ } \mu\text{m}$ (He I $4d^3D - 3p^3P$) and $2.06 \text{ } \mu\text{m}$ (He I $2p^1P - 2s^1S$ and He I $7d^3D - 4p^3P$). The determination of the terminal wind velocity is considerably facilitated by fitting both H - and K -band spectra. Now we can use two lines with P-Cygni like profiles. As each of both lines gives a slightly different range for v_∞ , the real value can be constrained to the overlap of both intervals.

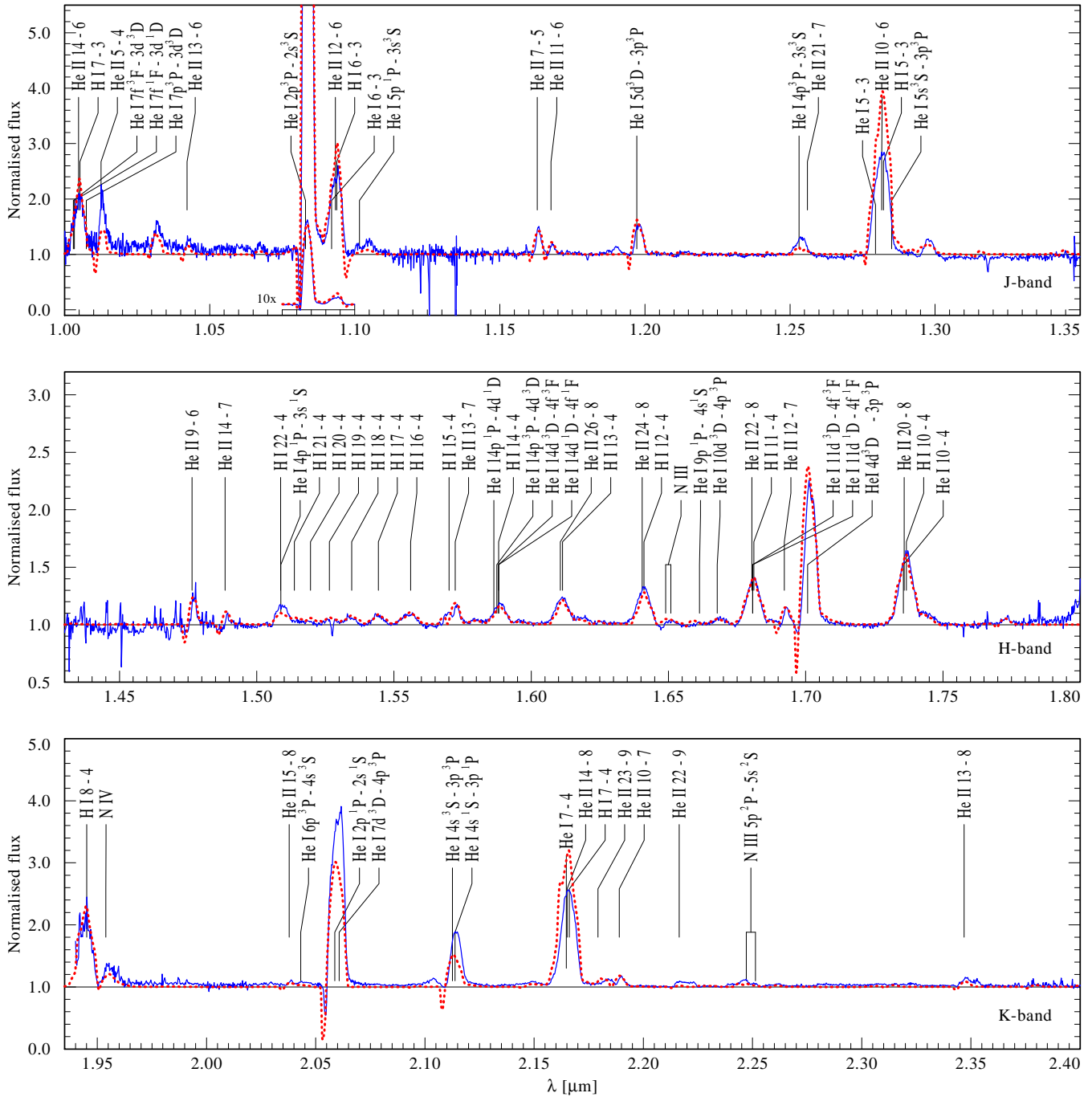


Figure 3. Observed *J*, *H*, and *K*-band spectra (blue-solid line) of WR 120bc, compared with the best-fitting model (red-dotted line) as in Fig. 2

As the spectra of WR 120bb and WR 120bc look very similar the best-fitting models have nearly identical parameters (Table 3).

The stellar temperature is adjusted such that the balance between the lines from He I versus He II is reproduced. The He II 7-5 line at $1.16 \mu\text{m}$ in the *J*-band and the He II 9-6 line at $1.48 \mu\text{m}$ in the *H*-band are the most important indicators for the determination of the temperature.

This is important to keep in mind, because there are

other parameter combinations with much lower temperatures which give well fitting model spectra as well, but only models with high temperatures of about 63 kK can reproduce the strengths of these He II lines.

At the same time, R_t is adjusted, which influences the strength of the emission lines in general.

The hydrogen to helium ratio is derived from fitting the line strengths of the Brackett series in the *H*-band. As there are few strong hydrogen lines in the *K*-band, the anal-

Table 3. Stellar parameters for WR 120bb and WR 120bc.

Stellar parameters	WR 120bb	WR 120bc
Spectral type	WN9h	WN9h
T_* [kK]	63 ± 2	63 ± 2
$\log R_t [R_\odot]$	0.36 ± 0.01	0.37 ± 0.01
$\log L [L_\odot]^\dagger$	5.66	5.54
$v_\infty [\text{km s}^{-1}]$	750 ± 50	750 ± 50
D	10	10
R_* [R_\odot] †	5.7	4.9
$\log \dot{M} [M_\odot \text{yr}^{-1}]^\dagger$	-4.4	-4.5
$\log \Phi_i [\text{s}^{-1}]$	48.6	48.6
$R_{2/3} [R_*]$	3.6	3.4
$T_{2/3} [\text{kK}]$	33 ± 2	34 ± 2
$E_{B-V} [\text{mag}]$	5.0	4.7
$A_{K_S} [\text{mag}]$	2.0	1.8
R_V	3.4	3.4
$M_{K_S} [\text{mag}]$	-6.7	-6.4
d [kpc] (adopted)	5.8	5.8
He [per cent by mass]	73 ± 5	73 ± 5
H [per cent by mass]	25 ± 5	25 ± 5
N [per cent by mass]	1.5	1.5
C [per cent by mass]	0.01	0.01
Fe [per cent by mass]	0.14	0.14

† The error margins of L , R_* and \dot{M} due to the spectral analysis are small, but their values scale with the adopted distance d which is less certain (see Sect. 4.3).

ysis of the H -band, which contains most of the Brackett-series, was essential to determine the hydrogen abundance. For the other elements, there were only weak and no unblended lines, so that we could not determine their abundances. That is why for other elements mass fractions which are typical for Galactic WN stars – N: 1.5, C: 0.01, Fe: 0.14 per cent (Hamann & Gräfener 2004) – are adopted.

The parameters from the best-fitting model for WR 120bb and WR 120bc are compiled in Table 3. The stellar temperature of 63 kK is unusually high for subtypes as late as WN9. As shown in Fig. 4, the domains of the WN subtypes in the $T_* - R_t$ -plane have a slope. Usually, the WN stars with late subtype and hydrogen are located at large R_t , i.e. their winds are relatively thin (see Hamann, Gräfener, & Liermann 2006). Our programme stars, however, show very thick winds (small R_t). Their location in the $T_* - R_t$ -diagram is consistent with the WN9 subtype derived above (Section 4.1) which is based on line ratios. However, with the unusually high density in the wind, higher stellar temperatures are required to reproduce the observed amount of ionised helium.

In addition, one should remember that T_* refers by definition to the radius R_* where the radial Rosseland optical depth reaches 20. This point of the atmosphere is of course not directly seen from outside. The observable photosphere is rather located at $R_{2/3}$ where the Rosseland optical depth has dropped to $2/3$. The winds of our program stars are so thick that $R_{2/3}/R_*$ is as large as 3.6 and 3.4, respectively (see Table 3). The effective temperature related to that radius is only $T_{2/3} = 33$ or 34 kK. Thus the location of R_* depends on the model assumption that the β -law for the velocity continues in the optically thick part of the expand-

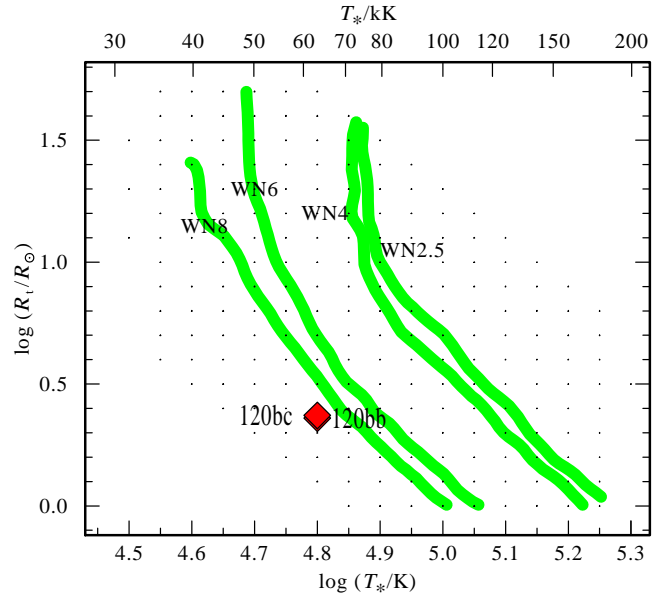


Figure 4. The positions of WR 120bb and WR 120bc (overlapping diamonds) in the $\log R_t - \log T_*$ diagram. The thick lines indicate where the classification criteria for selected subtypes (labels) match the line ratios that are predicted from theoretical models. The underlying model grid was calculated with the PoWR code (see Hamann & Gräfener 2004, for details).

ing atmosphere, albeit this cannot be observed, and has no influence on the spectral modelling.

4.3 Luminosity and distance of WR 120bb and WR 120bc

The absolute dimensions of the observed stars cannot be determined by spectral analysis only. They are related to the distance of the objects which is a priori unknown for WR 120bb and WR 120bc. Therefore, additional assumptions about the distance or the absolute magnitude have to be made in order to determine the luminosity, the stellar radius and the mass-loss rate.

The sightline towards WR 120bb and WR 120bc ($l \approx 28^\circ$) intersects the Sagittarius Arm (located at ~ 1.5 kpc from the Sun) and then (at ~ 3 kpc) enters into the Scutum-Centaurus (or Scutum-Crux) Arm (e.g. Churchwell et al. 2009). At a distance of ~ 6 kpc the sightline crosses a region of intense star formation (Garzon et al. 1997), which is located in the place where the Scutum-Centaurus Arm meets the receding tips of the Galactic traditional and long bars (Hammersley et al. 2000; Cabrera-Lavers et al. 2008; Churchwell et al. 2009). This region spans the Galactic latitude range from $\sim 24^\circ$ to 32° and contains numerous very massive clusters of red supergiants (Figer et al. 2006; Davies et al. 2007; Clark et al. 2009; Alexander et al. 2009; Negueruela et al. 2010, 2011; González-Fernández & Negueruela 2012) and the giant H II region W43 with a deeply embedded ($A_V \sim 30$ mag) cluster (named in the SIMBAD data base as [BDC99] W43 cluster), which contains at least three evolved massive stars (the WN7+a/OB? star WR 121a and two O-

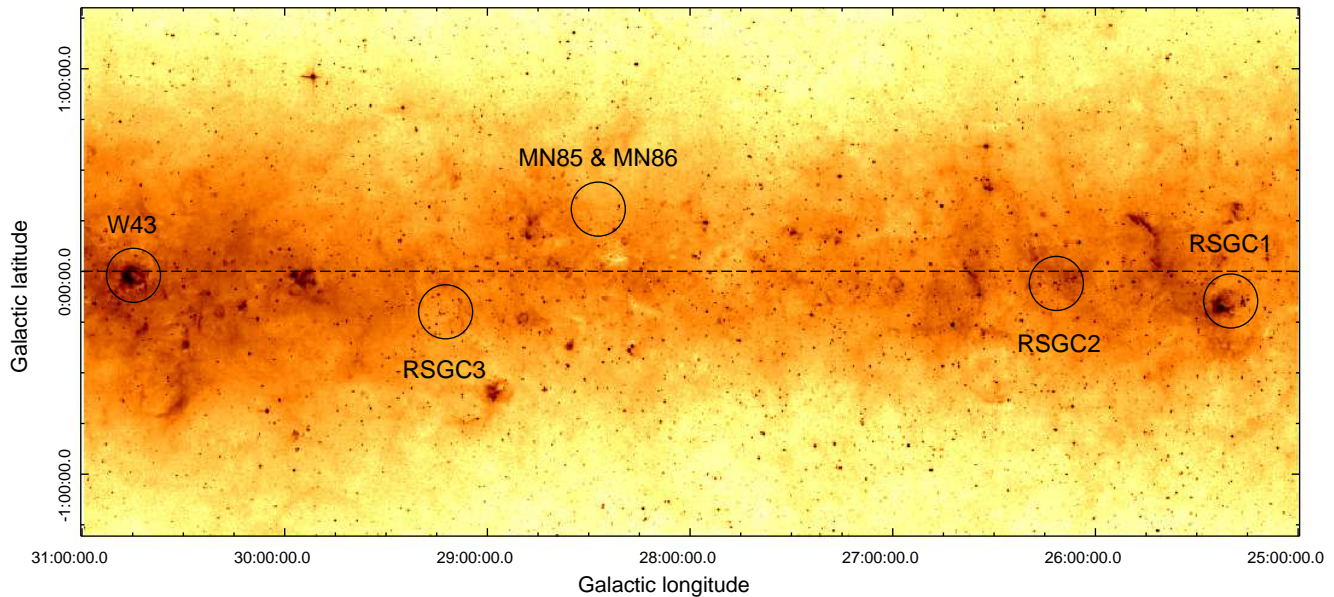


Figure 5. *MSX* 8.3 μm image of the Galactic plane centred at $l = 28^\circ, b = 0^\circ$. The positions of three red supergiant clusters (RSGC1,2,3), the central cluster of the giant H II region W43, and the cluster associated with WR 120bb and WR 120bc are indicated by circles. The Galactic plane is shown by a dashed line. See text for details.

type giants or supergiants; Blum, Daminieli, & Conti 1999)⁴. Fig. 5 shows the *Midcourse Space Experiment* (*MSX*) satellite (Price et al. 2001) image of a region of the Galactic plane centred at $l = 28^\circ, b = 0^\circ$, with the positions of three red supergiant star clusters, RSGC1 (Figer et al. 2006), RSGC2 (Davies et al. 2007), and RSGC3 (Clark et al. 2009; Alexander et al. 2009), the central cluster of the giant H II region W43 (Blum et al. 1999), and the cluster associated with WR120bb and WR120bc (Mauerhan et al. 2010) indicated by circles.

To constrain the distance to WR 120bb and WR 120bc, we may adopt plausible values for their absolute magnitude in the K -band. For eleven WN8-9h stars in the Arches cluster, located at the known distance of the Galactic center, Martins et al. (2008) obtained a mean K magnitude of -6.5 mag with an individual scatter between -6.8 and -5.8 mag⁵. However, these WN stars in the Arches cluster might be not representative for the stars discussed here, since the former are very luminous, but have relatively low mass loss rates which reduces their IR excess.

The calibration of M_{K_s} for Galactic WN stars by Crowther et al. (2006) suggests for WN7-9 stars a much smaller value of -5.9 mag. This value is the mean for only

three stars, whose parent clusters and associations are believed to be known. It is, however, strongly biased by the WN8(h)+cc? star WR66, which is either located at a larger distance than implied from its possible membership in the anonymous association in Circinus (Lundstrom & Stenholm 1984), or is a special case of a low-luminosity WN star originating from the binary channel. Without this star, the mean M_{K_s} for the remaining two (WN7h and WN9h) stars is -6.44 mag, which agrees well with our choice.

Adopting $M_K = -6.5$ mag and using the K_s -band extinction derived from the spectral energy distribution (SED) fitting (see below), we get distances of $d = 5.4$ kpc for WR 120bb and $d = 6.2$ kpc for WR 120bc, which imply that the stars are located in the Scutum-Centaurus Arm and that the radial separation between them is 0.8 kpc. Such a large separation, however, is less likely because both stars are probably members of a recently discovered star cluster (Mauerhan et al. 2010) and therefore are most likely spatially associated with each other. As M_K of the WN8-9h stars in the Arches cluster span quite a wide range, we assumed for both stars a common intermediate distance of $d = 5.8$ kpc. The corresponding stellar radii, mass-loss rates, luminosities, and absolute magnitudes are included in Table 3. For the sake of completeness we also give in Table 3 the hydrogen ionising luminosity, Φ_1 .

Table 3 shows that the stellar parameters we obtained are very similar for both stars. However, the reddening towards WR 120bb and WR 120bc is quite different. This difference can be caused by the non-uniform extinction across the cluster, e.g. due to inhomogeneities in the remainder of the parent molecular cloud. Alternatively, the enhanced reddening could be caused by a dense clump of the circumstellar shell projected along the line of sight towards WR 120bb (cf. Gvaramadze 2001).

⁴ The large ionising flux of the W43 star-forming region ($\sim 10^{51}$ Lyman continuum photons s^{-1} ; Smith, Biermann, & Mezger 1978) is comparable to that of the very massive ($\sim 10^4 M_\odot$) star cluster NGC 3603, which suggests that the central cluster in W43 contains a large number of yet undetected massive stars.

⁵ Note that these magnitudes were derived under the assumption of a uniform extinction across the Arches cluster of $A_K = 2.8$ mag, while it actually ranges from ≈ 2 to 4 mag (Espinoza, Selmán, & Melnick 2009). Thus, the actual range of M_K for WN8-9h stars remains unclear.

The observed SED was then fitted for each star (constructed from the flux-calibrated spectra and the photometric observations from DENIS, 2MASS, IRAC and *WISE*) with the model SEDs (Fig. 6) by adjusting the parameters of the reddening curve. For an appropriate treatment of the interstellar extinction, we adopted the reddening law from Fitzpatrick (1999), which covers the wavelength range up to 50 000 Å and allows adjustment of two parameters: the colour excess E_{B-V} and the total-to-selective absorption ratio $R_V = A_V/E_{B-V}$, which is 3.1 for the diffuse interstellar medium but can vary in general between 2.2 and 5.8 (Fitzpatrick 1999). For wavelengths above 50 000 Å, the reddening law from Moneti et al. (2001) is used. For the distance of $d = 5.8$ kpc for both stars, good fits to their SEDs are achieved with the parameters as given in Table 3. The excess seen at 22 μm obviously reflects the emission from dust, since the PSF of the *WISE* instrument (FWHM = 12'') covers a part of the circumstellar nebula.

The adopted distance to WR 120bb and WR 120bc of 5.8 kpc implies that the parent cluster of these stars is located near the base of the Scutum-Centaurus Arm, i.e. in the region of active star formation caused by the interaction between the Galactic bar(s) and the Galactic disk (Garzon et al. 1997). This inference is supported by a study of the distribution of interstellar extinction around $l \approx 28^\circ$, which shows that A_{K_s} slowly increases from 1.2 to 1.6 between 5–6 kpc, and then abruptly increases to 2–2.5 mag between 6 and 7 kpc (Negueruela et al. 2011, and references therein). Note that A_{K_s} towards WR 120bb and WR 120bc is comparable to that measured in the direction of the red supergiant clusters ($\approx 1.5 \pm 0.3$ mag). Since it is believed that all these clusters are located at a common distance of ~ 6 kpc (e.g. Clark et al. 2009; Negueruela et al. 2011), just in front of the large extinction wall, it is likely that the parent cluster of WR 120bb and WR 120bc is located at the same distance as well.

The actual distance to WR 120bb and WR 120bc, however, could differ from 5.8 kpc. It would be somewhat smaller (for the given M_K) if the circumcluster medium significantly contributes to the reddening of these stars. In this connection we note that A_{K_s} towards the cluster embedded in W43 (which is located at $d \sim 6$ kpc) is ~ 3 mag (Blum et al. 1999). Moreover, the absolute K -band magnitudes of WR 120bb and WR 120bc can differ from those given in Table 3. Assuming that they are in the same range as those of the WN8–9h stars in the Arches cluster (i.e. $-6.8 \dots -5.8$ mag; Martins et al. 2008), one finds that the distance to WR 120bb and WR 120bc can range from ~ 4.0 to 7.0 kpc, i.e. both stars are still located in the Scutum-Centaurus Arm. Correspondingly, the luminosities of WR 120bb and WR 120bc and their R_* and \dot{M} (given in Table 3) can be scaled to different distances as $\propto d^2$, $\propto d$, and $\propto d^{3/2}$, respectively (Schmutz, Hamann, & Wessolowski 1989).

5 PROGENITORS OF WR 120BB AND WR 120BC AND THE ORIGIN OF THEIR CIRCUMSTELLAR NEBULAE

The luminosity of WR 120bb and WR 120bc of $\log(L/L_\odot) \approx 5.5 - 5.7$ (derived for our preferred distance of 5.8 kpc) implies that the initial (zero-age main-sequence) masses of

these stars were $\lesssim 40 M_\odot$ (e.g. Ekström et al. 2012). A massive star of this mass evolves through the sequence: MS (main sequence) \rightarrow RSG (red supergiant) \rightarrow WN, and ends its life in a type II supernova. During the MS phase the star creates an extended (tens of pc) bubble filled with hot, tenuous gas (e.g. Weaver et al. 1977). Then, during the RSG phase it loses a considerable fraction of its initial mass in the form of slow, dense wind, which occupies a compact (a few pc) region of enhanced density within the MS bubble. This region is surrounded by a dense shell, which is created by the high-pressure interior of the MS bubble acting on the expanding RSG wind, so that the radius of the shell, r_{RSG} , is determined by the balance between the ram pressure of the RSG wind and the thermal pressure in the interior of the MS bubble (e.g. D’Ercole 1992):

$$\frac{\dot{M}_{\text{RSG}} v_{\text{RSG}}}{4\pi r_{\text{RSG}}^2} \approx \frac{7}{(3850\pi)^{2/5}} L_{\text{MS}}^{2/5} \rho_0^{3/5} t^{-4/5}, \quad (2)$$

where \dot{M}_{RSG} and v_{RSG} are, respectively, the mass-loss rate and the wind velocity during the RSG phase, L_{MS} is the mechanical luminosity of the stellar wind during the MS phase, $\rho_0 = 1.4 m_{\text{H}} n_0$, m_{H} is the mass of a hydrogen atom, and n_0 is the number density of the ambient interstellar medium. Since WR 120bb and WR 120bc are members of the cluster containing (at least) two other evolved massive stars (whose progenitors were nearly as massive as those of WR 120bb and WR 120bc), it is likely that all these stars contribute to the thermal pressure of the common bubble around the cluster.

Adopting $\dot{M}_{\text{RSG}} = 3 \cdot 10^{-5} M_\odot \text{yr}^{-1}$ and $v_{\text{RSG}} = 15 \text{ km s}^{-1}$ (the figures typical of RSGs), and assuming $L_{\text{MS}} = 3 \cdot 10^{36} \text{ erg s}^{-1}$ and $n_0 = 1 \text{ cm}^{-2}$, one has from equation (2) that at the beginning of the WR phase (i.e. at $t \gtrsim 4$ Myr)

$$r_{\text{RSG}} \approx 3 \text{ pc} \left(\frac{\dot{M}_{\text{RSG}}}{10^{-5} M_\odot \text{yr}^{-1}} \right)^{1/2} \left(\frac{v_{\text{RSG}}}{15 \text{ km s}^{-1}} \right)^{1/2} \cdot \left(\frac{L_{\text{MS}}}{3 \cdot 10^{36} \text{ erg s}^{-1}} \right)^{-1/5} \left(\frac{n_0}{1 \text{ cm}^{-3}} \right)^{-3/10} \left(\frac{t}{4 \text{ Myr}} \right)^{2/5},$$

which is comparable to the linear radii of the shells MN85 and MN86 ($r_{\text{sh}} \sim 3$ pc; see Section 2).

The subsequent fast WR wind sweeps up the RSG wind and creates a new shell, which expands through the region occupied by the RSG wind with a constant velocity (e.g. Chevalier & Imamura 1983; D’Ercole 1992)

$$v_{\text{sh}} \approx \left(\frac{\dot{M}_{\text{WR}} v_{\text{WR}}^2}{3 \dot{M}_{\text{RSG}}} \right)^{1/3}, \quad (3)$$

where \dot{M}_{WR} and v_{WR} are, respectively, the mass-loss rate and the wind velocity during the WR phase. With \dot{M}_{WR} and v_{WR} from Table 3, one has from equation (3) $v_{\text{sh}} \approx 160 \text{ km s}^{-1}$, which in turn gives the dynamical age of the shells of $t_{\text{dyn}} \sim r_{\text{sh}}/v_{\text{sh}} \sim 2 \cdot 10^4 \text{ yr}$. Note that v_{sh} and t_{dyn} only weakly depend on the distance (both $\propto d^{1/2}$). The small dynamical age of the shells implies that WR 120bb and WR 120bc entered the WR phase only recently, which is consistent with the observational fact that WR circumstellar nebulae are associated exclusively with WNL stars (Gvaramadze et al. 2009, 2010a, and references therein), i.e. with very young WR stars, whose winds still interact with

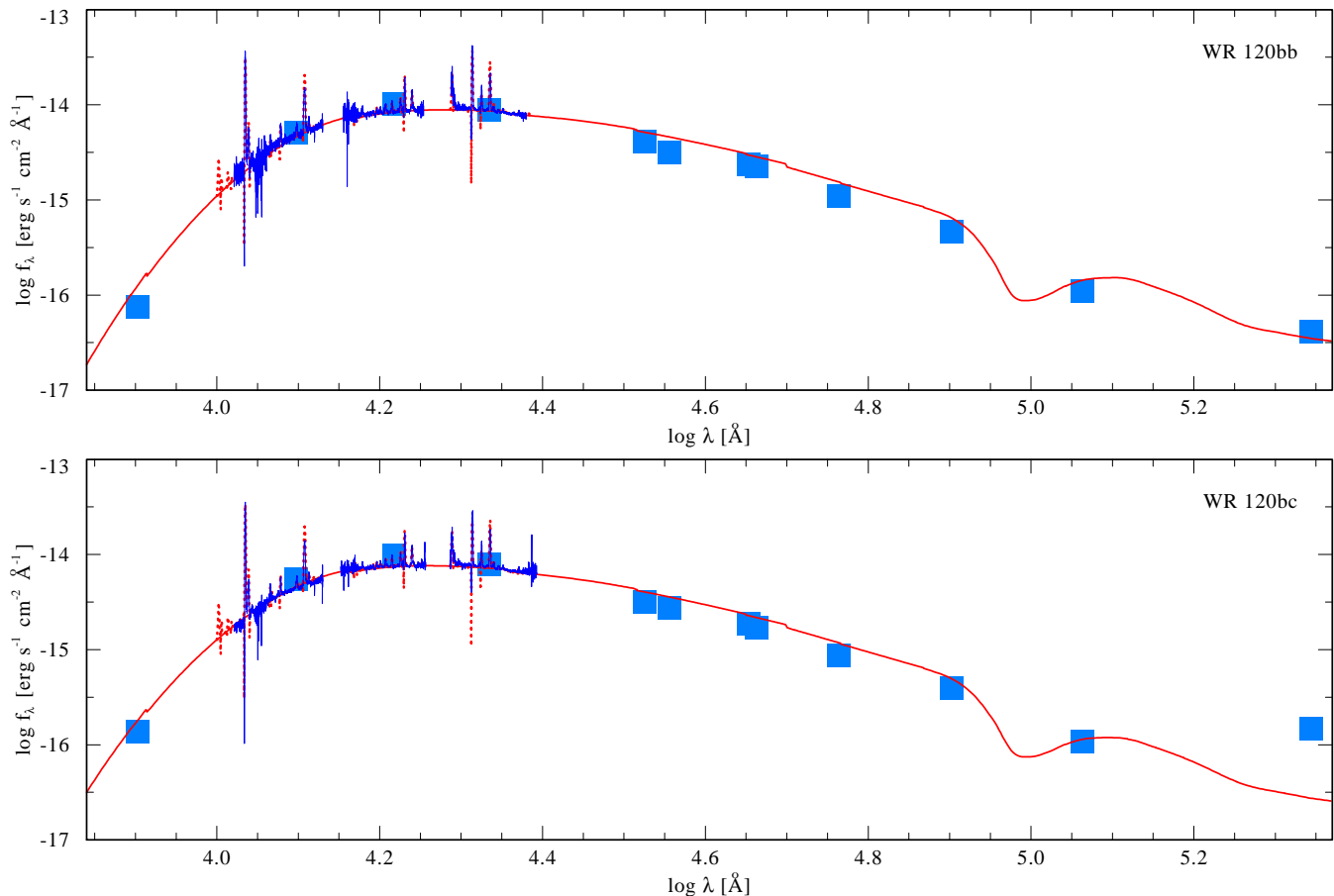


Figure 6. Observed flux distribution of WR120bb and WR120bc (blue line) in absolute units, including the calibrated spectrum and the photometric measurements compiled in Table 1, compared to the emergent flux of the model continuum (red/smooth line), in the infrared also shown with spectral lines (red/dotted line). The model flux has been reddened and scaled to the distance according to the parameters given in Table 3.

the dense circumstellar medium. On the other hand, the small size of the region occupied by the RSG wind implies that the circumstellar shells around WR stars are short-lived (several tens of thousands of years; e.g. van Marle, Langer, & García-Segura 2005) objects.

6 SUMMARY

We analysed new J , H , and K -band spectra of two neighbouring optically obscured Wolf-Rayet stars, WR 120bb and WR 120bc, which were revealed via detection of their (apparently interacting) circumstellar shells with the *Spitzer Space Telescope* and follow-up spectroscopy of central stars of the shells. Our analysis of the spectra was based on the use of the Potsdam Wolf-Rayet model atmosphere code, whose atomic data base has been extended in order to include all significant lines in the near-infrared bands. It is shown that the use of the J - and H -band is of great additional value for the analysis compared to an analysis which is based on the K -band spectrum alone. Despite the late spectral subtype of WR 120bb and WR 120bc, we found relatively high stellar temperatures of 63 kK for both stars. The stellar wind composition is dominated by helium with 25 per cent of hydrogen. The stellar spectra are significantly reddened, $A_{K_s} \approx 2$

mag, which is consistent with the location of the stars in the Scutum-Centaurus arm. Adopting a common distance of 5.8 kpc, WR 120bb and WR 120bc have luminosities of $\log(L/L_\odot) = 5.66$ and 5.54 and mass-loss rates of $10^{-4.4}$ and $10^{-4.5} M_\odot \text{ yr}^{-1}$, respectively. These values have to be considered as highly uncertain due to the uncertainty of the adopted distance. The inferred luminosities imply that the immediate precursors of WR 120bb and WR 120bc were red supergiant stars of initial mass of $\lesssim 40 M_\odot$, which in turn implies that the circumstellar shells around both stars originate because of interaction between the Wolf-Rayet wind and the dense material shed during the preceding red supergiant phase.

7 ACKNOWLEDGEMENTS

We are grateful to the referee for a careful reading of the manuscript and comments that allowed us to improve the content of the paper. Observations presented were obtained with the Apache Point Observatory 3.5-meter telescope, which is owned and operated by the Astrophysical Research Consortium. A.Y.K acknowledges the support from the National Research Foundation (NRF) of South Africa. This work has made use of the NASA/IPAC Infrared Science

Archive, which is operated by the Jet Propulsion Laboratory, California Institute of Technology, under contract with the National Aeronautics and Space Administration, the SIMBAD database and the VizieR catalog access tool, both operated at CDS, Strasbourg, France.

References

- Alexander M. J., Kobulnicky H. A., Clemens D. P., Jameson K., Pinnick A., Pavel M., 2009, *AJ*, 137, 4824
- Barniske A., Oskinova L. M., Hamann W.-R., 2008, *A&A*, 486, 971
- Benjamin R. A. et al., 2003, *PASP*, 115, 953
- Blum R. D., Damineli A., Conti P. S., 1999, *AJ*, 117, 1392
- Cabrera-Lavers A., González-Fernández C., Garzón F., Hammersley P. L., López-Corredoira M., 2008, *A&A*, 491, 781
- Carey S. J. et al., 2009, *PASP*, 121, 76
- Chevalier R. A., Imamura J. N., 1983, *ApJ*, 270, 554
- Chu Y.-H., Treffers R. R., Kwitter K. B., 1983, *APJS*, 53, 937
- Churchwell E. et al., 2009, *PASP*, 121, 213
- Clark J. S., Egan M. P., Crowther P. A., Mizuno D. R., Larionov V. M., Arkharov A., 2003, *A&A*, 412, 185
- Clark J. S. et al., 2009, *A&A*, 498, 109
- Crowther P. A., Hadfield L. J., Clark J. S., Negueruela I., Vacca W., 2006, *MNRAS*, 372, 1407
- Cushing M. C., Vacca W. D., Rayner J. T., 2004, *PASP*, 116, 362
- Cutri R. M. et al., 2003, *VizieR Online Data Catalog*, 2246, 0
- Cutri R. M. et al., 2012, *VizieR Online Data Catalog*, 2311, 0
- Davies B., Figer D. F., Kudritzki R.-P., MacKenty J., Najarro F., Herrero A., 2007, *ApJ*, 671, 781
- D’Ercole A., 1992, *MNRAS*, 255, 572
- Dopita M. A., Bell J. F., Chu Y.-H., Lozinskaya T. A., 1994, *APJS*, 93, 455
- Egan M. P., Clark J. S., Mizuno D. R., Carey S. J., Steele I. A., Price S. D., 2002, *ApJ*, 572, 288
- Ekström S. et al., 2012, *A&A*, 537, A146
- Espinoza P., Selman F. J., Melnick J., 2009, *A&A*, 501, 563
- Fazio G. G. et al., 2004, *APJS*, 154, 10
- Figer D. F., MacKenty J. W., Robberto M., Smith K., Najarro F., Kudritzki R. P., Herrero A., 2006, *ApJ*, 643, 1166
- Fitzpatrick E. L., 1999, *PASP*, 111, 63
- Flagey N., Noriega-Crespo A., Billot N., Carey S. J., 2011, *ApJ*, 741, 4
- Garzon F., Lopez-Corredoira M., Hammersley P., Mahoney T. J., Calbet X., Beckman J. E., 1997, *APJL*, 491, L31
- González-Fernández C., Negueruela I., 2012, *A&A*, 539, A100
- Gräfener G., Koesterke L., Hamann W.-R., 2002, *A&A*, 387, 244
- Gvaramadze V. V., 2001, *A&A*, 374, 259
- Gvaramadze V. V., Chené A., Kniazev A. Y., Schnurr O., 2011, *ArXiv e-prints* 1110.0126
- Gvaramadze V. V. et al., 2009, *MNRAS*, 400, 524
- Gvaramadze V. V., Kniazev A. Y., Fabrika S., 2010a, *MNRAS*, 405, 1047
- Gvaramadze V. V., Kniazev A. Y., Fabrika S., Sholukhova O., Berdnikov L. N., Cherepashchuk A. M., Zharova A. V., 2010b, *MNRAS*, 405, 520
- Gvaramadze V. V., Kniazev A. Y., Hamann W.-R., Berdnikov L. N., Fabrika S., Valeev A. F., 2010c, *MNRAS*, 403, 760
- Hadfield L. J., van Dyk S. D., Morris P. W., Smith J. D., Marston A. P., Peterson D. E., 2007, *MNRAS*, 376, 248
- Hamann W.-R., Feldmeier A., Oskinova L. M., eds., 2008, *Clumping in hot-star winds*
- Hamann W.-R., Gräfener G., 2003, *A&A*, 410, 993
- Hamann W.-R., Gräfener G., 2004, *A&A*, 427, 697
- Hamann W.-R., Gräfener G., Liermann A., 2006, *A&A*, 457, 1015
- Hammersley P. L., Garzón F., Mahoney T. J., López-Corredoira M., Torres M. A. P., 2000, *MNRAS*, 317, L45
- Helfand D. J., Becker R. H., White R. L., Fallon A., Tuttle S., 2006, *AJ*, 131, 2525
- Johnson H. M., Hogg D. E., 1965, *ApJ*, 142, 1033
- Kramida A., Ralchenko Y., Reader J., NIST ASD Team, 2012, access via <http://physics.nist.gov/asd>
- Liermann A., Hamann W.-R., Oskinova L. M., Todt H., Butler K., 2010, *A&A*, 524, A82
- Lundstrom I., Stenholm B., 1984, *AAPS*, 58, 163
- Marston A. P., 1991, *ApJ*, 366, 181
- Marston A. P., 1995, *AJ*, 109, 1839
- Martins F., Hillier D. J., Paumard T., Eisenhauer F., Ott T., Genzel R., 2008, *A&A*, 478, 219
- Mathis J. S., Cassinelli J. P., van der Hucht K. A., Prusti T., Wesselius P. R., Williams P. M., 1992, *ApJ*, 384, 197
- Mauerhan J. C., Van Dyk S. D., Morris P. W., 2011, *AJ*, 142, 40
- Mauerhan J. C., Wachter S., Morris P. W., Van Dyk S. D., Hoard D. W., 2010, *APJL*, 724, L78
- Mizuno D. R. et al., 2010, *AJ*, 139, 1542
- Moneti A., Stolovy S., Blommaert J., Figer D., Najarro F., 2001, *A&A*, 366, 106
- Negueruela I., González-Fernández C., Marco A., Clark J. S., 2011, *A&A*, 528, A59
- Negueruela I., González-Fernández C., Marco A., Clark J. S., Martínez-Núñez S., 2010, *A&A*, 513, A74
- Price S. D., Egan M. P., Carey S. J., Mizuno D. R., Kuchar T. A., 2001, *AJ*, 121, 2819
- Rieke G. H. et al., 2004, *APJS*, 154, 25
- Schmutz W., Hamann W.-R., Wessolowski U., 1989, *A&A*, 210, 236
- Shara M. M., Faherty J. K., Zurek D., Moffat A. F. J., Gerke J., Doyon R., Artigau E., Drissen L., 2012, *AJ*, 143, 149
- Shara M. M. et al., 2009, *AJ*, 138, 402
- Shara M. M., Moffat A. F. J., Smith L. F., Niemela V. S., Potter M., Lamontagne R., 1999, *AJ*, 118, 390
- Smith L. F., Biermann P., Mezger P. G., 1978, *A&A*, 66, 65
- Smith L. F., Shara M. M., Moffat A. F. J., 1996, *MNRAS*, 281, 163
- Stringfellow G. S., Gvaramadze V. V., Beletsky Y., Kniazev A. Y., 2011, *ArXiv e-prints* 1112.2686
- Stringfellow G. S., Gvaramadze V. V., Beletsky Y., Kniazev A. Y., 2012, in *IAU Symposium*, Vol. 282, *From Interacting Binaries to Exoplanets: Essential Modeling Tools*, Richards M. T., Hubeny I., eds., pp. 267–268

- The DENIS Consortium, 2005, VizieR Online Data Catalog, 2263, 0
- Trams N. R., Voors R. H. M., Waters L. B. F. M., 1998, APSS, 255, 195
- Vacca W. D., Cushing M. C., Rayner J. T., 2003, PASP, 115, 389
- van Buren D., McCray R., 1988, APJL, 329, L93
- van der Hucht K. A., 2001, New Astron. Rev, 45, 135
- van der Hucht K. A., 2006, A&A, 458, 453
- van Hoof P., 1999, access via <http://www.pa.uky.edu/peter/atomic/index.html>
- van Marle A. J., Langer N., García-Segura G., 2005, A&A, 444, 837
- Voors R. H. M. et al., 2000, A&A, 356, 501
- Wachter S., Mauerhan J., Van Dyk S., Hoard D., Kafka S., Morris P., 2010, AJ, 139
- Wachter S., Mauerhan J., van Dyk S., Hoard D. W., Morris P., 2011, Bulletin de la Societe Royale des Sciences de Liege, 80, 291
- Weaver R., McCray R., Castor J., Shapiro P., Moore R., 1977, ApJ, 218, 377
- Wilson J. C. et al., 2004, in Society of Photo-Optical Instrumentation Engineers (SPIE) Conference Series
- Wright E. L. et al., 2010, AJ, 140, 1868